BEAM DYNAMICS SIMULATION OF THE LAMPF LINEAR ACCELERATOR

R. W. Garnett, R. S. Mills, and T. P. Wangler
Los Alamos National Laboratory, Los Alamos, NM 87545*

Abstract

We performed an end-to-end simulation of the LAMPF linac to test the capability of our codes to predict the actual performance of an accelerator system. We attempted to reproduce the measured H^+ beam transverse emittances, and wire-scan, phase-scan and beam-loss data for a typical LAMPF operating cycle by using the known operating parameters of the linac. The simulations were also useful in understanding the beam dynamics of LAMPF and for explaining the sources of linac emittance growth and particle losses in the side-coupled linac.

Simulation Techniques

The LAMPF accelerator consists of a 0.75-MeV injector, with a low-energy beam transport (LEBT) line, a 0.75 to 100-MeV drift-tube linac (DTL), a 100-MeV transport line called the transition region (TR), and a 100 to 800-MeV side-coupled linac (SCL). The DTL incorporates singlet FODO focusing. The focusing period is doubled in the last two of four tanks by placing a quadrupole only in every other drift-tube. Doublet FDO focusing is used in the SCL. The number of particles per bunch is about 5 x 10^8, which gives a peak current of 15 mA at 201.25 MHz in the DTL. Because the physics of the LEBT is not well understood (the amount of beam neutralization is unknown and no measurements of the longitudinal beam structure are made), we decided to start the simulation at the entrance to tank 1 of the DTL, using longitudinal input distributions that represent different assumptions about the LEBT physics.

We simulated the DTL and TR using the PARMILA code. Two longitudinal input distributions were used. We obtained these distributions by propagating a beam in the LEBT, beginning with a truncated beam ($\pm 120°$) at the second of two bunchers, and ending at the entrance to the first tank of the DTL. The space-charge in PARMILA was set to zero for the first case to represent 100% neutralization and to a current of 17-mA for the second case. The first case was designated ZSC for zero space-charge in the LEBT and the second, SCD for space-charge dominated in the LEBT. In both cases, the transverse beam was regenerated at the DTL entrance as an rms matched Gaussian distribution (truncated at 3σ), which is consistent with the measured beam, and simulated at full current in the linac.

We believe that the longitudinal beam distribution is bracketed by these two extremes. Figure 1 shows longitudinal phase-space plots for these two distributions at both the entrance to the DTL (0.75-MeV) and the exit of the TR (100-MeV).

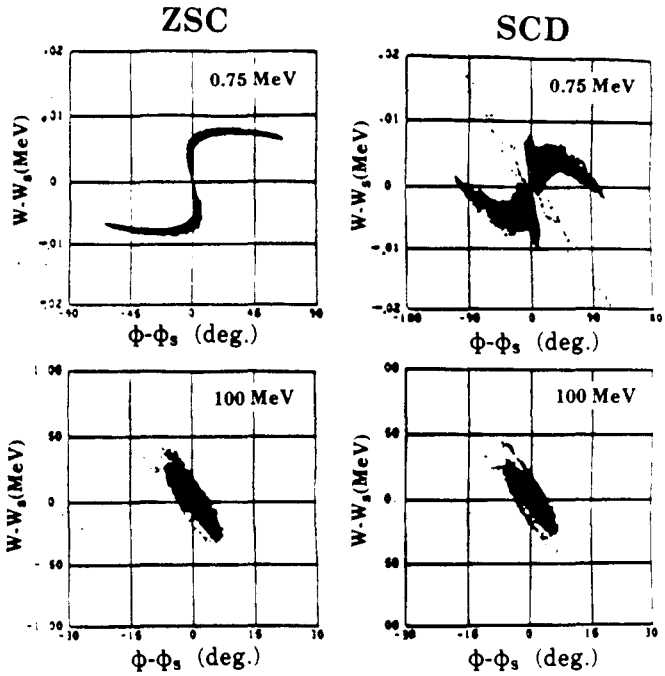

Fig. 1. Longitudinal phase-space plots for the two input distributions.

All simulations began with 10,000 pseudoparticles. The DTL r.f. amplitude in tank 1 is not accurately known and is purposely set below the maximum value for typical linac operation. In the simulations, the amplitude was set to 94% of the design value. This resulted in realistic transmissions through the DTL in the range of 72% to 80% for the various cases studied. We ran DTL simulations with both "design" and measured ("production") r.f. field gradients, quadrupole strengths, and cell lengths.

Output distributions from the PARMILA code simulations were used as input for the coupled-cavity code, CCLDYN. We used the SCL design values for r.f. field gradients and quadrupole strengths. Actual experimental settings for the last five quadrupoles in the DTL were used in all the DTL simulations to provide the experimental match to the CCL. Measured misalignments for tanks and magnets were not used.

At LAMPF, phase-scans done at 121-MeV in the SCL are used to determine the phase-width of the beam. An absorber-collector method is used. A copper absorber, placed in the beam with its thickness chosen so as to stop protons with kinetic energy (W) less than 117.42-MeV but to pass those with W>122.58-MeV, places a lower-limit energy cut-off on the phase-space to be scanned. In the phase-scan simulations, particles with energy less than 5-MeV below the synchronous energy were rejected in order to mock-up the effect of the

*Work supported by Los Alamos National Laboratory Institutional Supporting Research, under auspices of the United States Department of Energy.

absorber. We ran particle-loss simulations with both the SCD and ZSC input distributions. No energy cut was made as the particles propagated, consistent with actual accelerator operation.

Comparison of Simulation and Measurement

The results of experimental measurements for LAMPF operating cycle 52[1] are given in Table 1. All emittances are rms-normalized values but do not include the factor of four that is sometimes used. The table shows a difference between wire-scan and slit and collector data at 100-MeV; experimental measurement uncertainties, however, were not available. Table 2 shows the results of the simulations for comparison. The 100-MeV phase-space plots in Fig. 1 and the results in Table 2, show that the beam becomes conditioned in the DTL regardless of its initial longitudinal distribution and that the properties of the core beam particles are mostly determined by the DTL. By contrast, the outer parts of the distribution (the tails) appear to be sensitive to the input longitudinal distribution.

TABLE 1
LAMPF Cycle 52 Experimental Results

Measurement		Value
Particle Loss		~0.1%
Phase-Scan at 121 MeV (just after module 6)		FWHM ≃ 15.9°
Wire-Scan at 800 MeV for rms beam size		FWHM ≃ 0.54 cm
Emittance Measurements		
100 MeV	Slit & Collector	$\bar{\varepsilon}_t$ = 0.026 π-cm-mrad
	Wire Scan	$\bar{\varepsilon}_t$ = 0.053 π-cm-mrad
800 MeV	Wire Scan	$\bar{\varepsilon}_t$ = 0.071 π-cm-mrad

The simulations predict all measured quantities to within 10% to 15%, except the total SCL beam losses, which we expect to be sensitive to the population of the tails. At 100-MeV, the simulations agree best with the slit and collector measurements. The SCL beam losses are best predicted, to within a factor of 3, by using the "design" SCD distribution. Use of the "production" distributions overestimates the losses by about an order of magnitude. Additionally, the locations along the SCL where most of the activation occurs were correctly predicted by any of the input distributions. Figure 2a shows a typical beam loss profile from the simulations. Figure 2b sshows the estimated beam losses in the SCL from activation measurements.

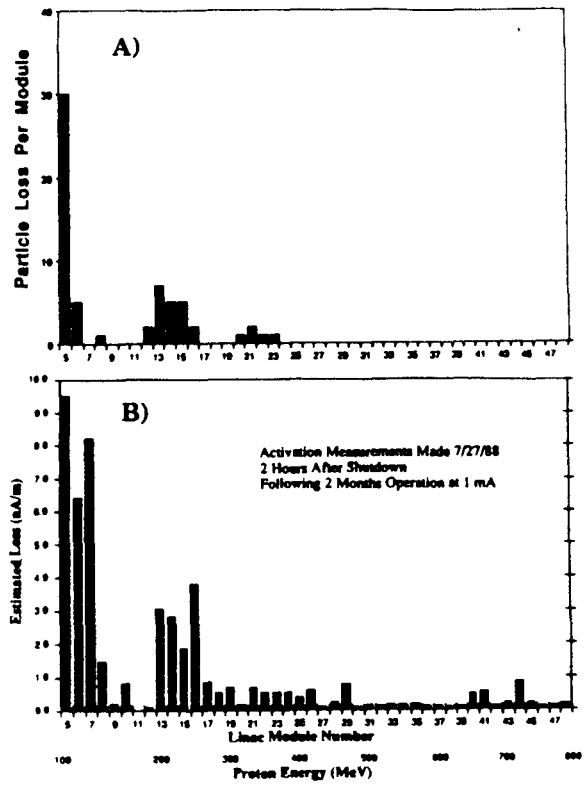

Fig. 2. Typical SCL beam-loss profile fromthe simulations. b) Estimated beam losses in the SCL from activation measurements.

TABLE 2
Results of LAMPF Simulation

Distribution Type	$\bar{\varepsilon}_t$ π-cm-mrad 100 MeV	$\bar{\varepsilon}_t$ π-cm-mrad 800 MeV	$\bar{\varepsilon}_\ell$ π-cm-mrad 100 MeV	$\bar{\varepsilon}_\ell$ π-cm-mrad 800 MeV	121 MeV Phase FWHM (deg.)	800 MeV Size FWHM (cm)	Losses (%)
"DESIGN" SCD	0.026	0.065	0.575	1.090	17.03	0.60	0.35
"DESIGN" ZSC	0.028	0.067	0.637	1.175	24.69	0.78	0.41
"PRODUCTION" SCD	0.030	0.065	0.659	1.240	17.41	0.67	0.98
"PRODUCTION" ZSC	0.032	0.063	0.725	1.091	22.26	0.75	1.76

LAMPF Losses and Longitudinal Emittance

While longitudinal emittance is not directly measured at LAMPF, phase-scans give a one-dimensional phase projection of two-dimensional longitudinal phase-space. When LAMPF is being tuned, the operators attempt to minimize particle losses by narrowing the phase-width. It is impossible to determine from the accelerator tuning procedures used by the LAMPF operators whether this narrowing is accomplished by their decreasing the longitudinal emittance of the beam or by rotating it in phase-space to give a minimum projection.

To study the correlation between longitudinal emittance (or phase-width) and losses, we transformed the "design" SCD distribution at 100 MeV to change the rms longitudinal emittance and thereby alter the phase-width. We found that the SCL losses are indeed a function of the longitudinal emittance with a sharp minimum at $\varepsilon_L = 0.497$ π-deg-MeV. This value of phase-width ($\Delta\phi = 15.7°$) is within 0.3° of the measured operating value, which gave minimum accelerator activation. The simulations showed that particles lost near tank 1 of the SCL (module 5) lie in the tails of the y-y' distribution but are close to the synchronous phase. Those particles that are eventually lost radially near tank 33 (module 13) have small initial transverse coordinates but are at the edge of the longitudinal acceptance.

Emittance Growth in the Linac

We compared PARMILA simulations of the DTL with and without the effect of space-charge forces. We determined that the transverse emittance growth in the DTL is caused by the non-linear space-charge forces acting on the beam. The longitudinal emittance growth was essentially unaffected. We believe that the longitudinal emittance growth is caused by the non-linear r.f. focusing forces encountered in the DTL. Figure 3 shows both the average-transverse and longitudinal emittances along the DTL. Asymmetries in x-x' and y-y' emittances were encountered in both the DTL and SCL simulations. This feature, although it is also observed in the measured emittance data, is not understood and therefore we make comparisons of the average of x-x' and y-y' emittances. Figure 3 shows that rapid transverse emittance growth is seen to occur in tank 2 and tank 3 (where the focusing period changes). The simulation shows particle losses throughout the DTL, which tends to cause some reduction in the emittances.

It is commonly believed that most emittance growth occurs in the low-energy end of a linac. The measured slit and collector data at 100-MeV indicate that the transverse emittance grows by a factor of 2.7 between 100 and 800-MeV at LAMPF. Our simulations gave values in the range 2.0-2.5.

We believe that the emittance growth in the SCL is primarily due to mismatch (mostly longitudinal) of the beam and is caused by the nonlinear space-charge forces acting on it. To verify our belief, we turned off the effect of r.f. defocus in the simulations. We observed no change in emittance growth. For comparison, the SCL emittance growth became negligible when the space-charge forces were turned off. Table 3 gives mismatch factors at 100-

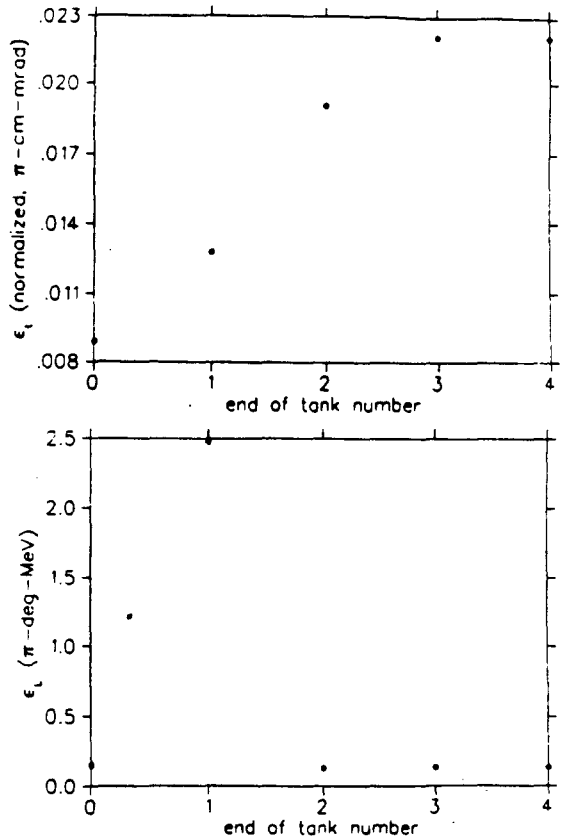

Fig. 3. Emittances as a function of tank number in the DTL from the simulations for the SCD beam. Longitudinal emittance is in units of π–deg–MeV at 201.25 MHz.

MeV calculated for both the SCD beam and the actual beam using the slit and collector data. The mismatch factor[2] is defined by

$$M = \left[\frac{1}{2}R + \frac{1}{2}\sqrt{R^2 - 4}\right]^{1}_{2} - 1$$

where $R = \beta_1\gamma_2 + \beta_2\gamma_1 - 2\alpha_1\alpha_2$ and α_i, β_i, γ_i $(i = 1,2)$ are the Twiss parameters for the matched and unmatched ellipses. For a matched beam, M = 0.

TABLE 3
Mismatch Factors at 100 MeV

Distribution	M_x	M_y	M_L
"Design" SCD	0.155	0.896	1.381
Measured Slit and Collector	0.388	0.587	–

Figure 4 shows both the average-transverse and longitudinal emittances as functions of tank number along the SCL for the "design" SCD

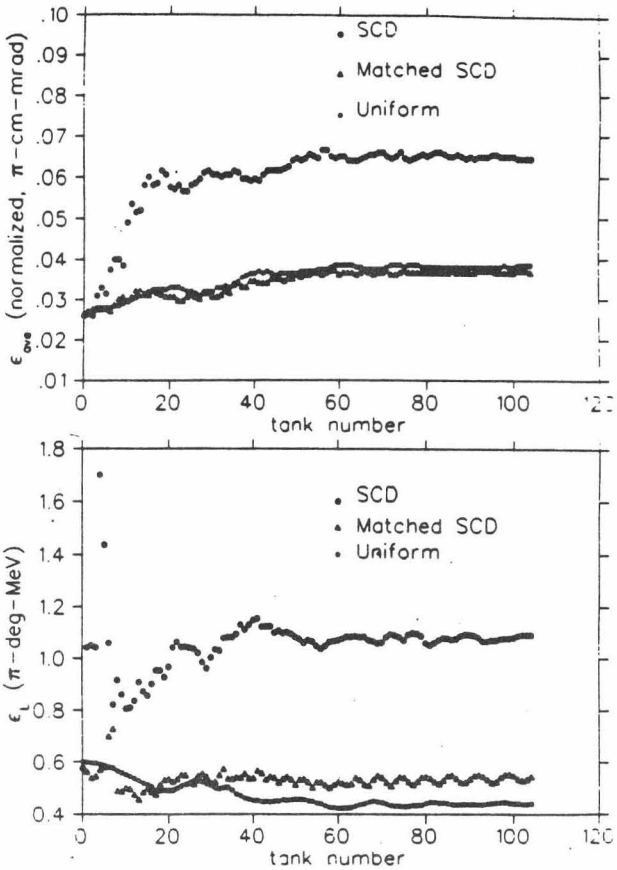

Fig. 4. SCL emittances for unmatched SCD, matched SCD, and uniform input distributions. Longitudinal emittance is in units of π–deg–MeV at 805 MHz.

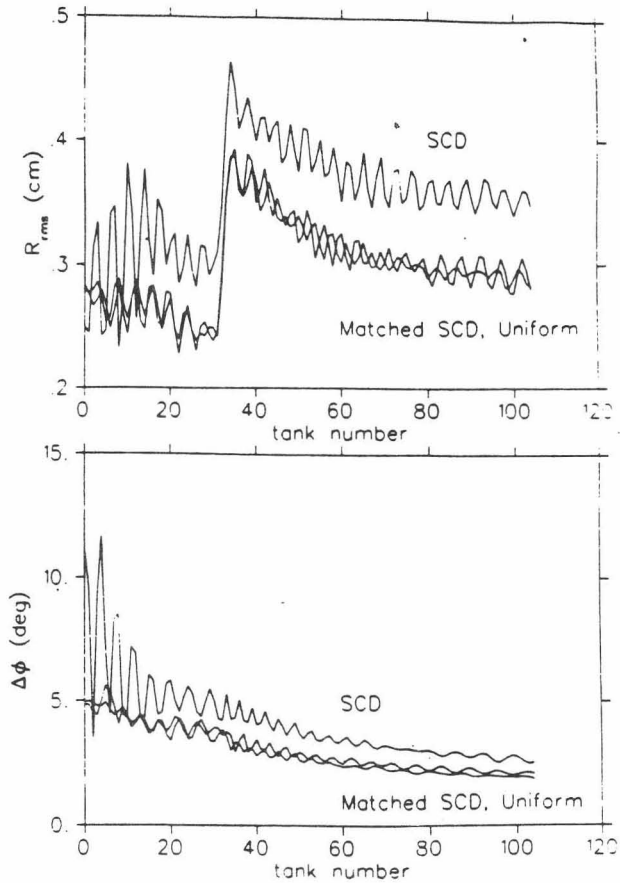

Fig. 5. Transverse and longitudinal rms beam sizes for the SCD and uniform beam in the SCL (R rms = $\sqrt{X3 + Y2rms}$).

distribution. Also shown are curves for an rms-matched SCD distribution and a matched uniform distribution (uniform ellipsoid in real space and approximately uniform in velocity space).

We created a matched SCD distribution by transforming the coordinates of each particle of the "design" SCD distribution at 100 MeV such that the new distribution had Twiss parameters identical to those obtained from TRACE-3D[3] for an rms match at the input to the SCL. The initial emittances of the distribution were preserved.

Figure 4 shows that there is a drastic reduction in emittance growth, both transversely and longitudinally, if the beam is rms-matched to the linac. The matched beam behaves very much like the uniform beam, which is evident in both the emittances and rms beam sizes (Fig. 5). The observed increase in transverse rms beam size near tank 33 (module 13) is due to a reduction in quadrupole focusing strength at this point in the linac. The average quadrupole gradients and lengths remain constant at about 25 T/m and 0.1 m, respectively, but the tank lengths, and therefore the quadrupole spacings, approximately double. A factor-of-5 reduction in beam losses was also observed in the simulations for the matched beam. This is probably due to the reduction in synchrotron oscillation amplitude at the entrance to the SCL. This energy would otherwise later couple to the transverse degrees of freedom and cause particle losses further downstream in the linac.

Both longitudinal and transverse emittance growth are still observed for the ideal matched SCD and uniform beams. Figure 4 clearly indicates a coupling between transverse and longitudinal degrees of freedom. The longitudinal emittance decreases as the transverse emittance grows. We believe that this relationship is due to a lack of equipartitioning of the matched beam in the SCL. RMS matching and equipartitioning should result in a beam that more closely resembles an internally matched beam and should therefore reduce the space-charge-induced emittance growth.

Acknowledgments

We would like to thank J. Hurd and A. Browman of the LAMPF operations group for their interest and for providing us with the experimental data. Also, we would like to thank K. R. Crandall, G. P. Lawrence, S. Nath, and G. H. Neuschaefer for their help in this study.

References

1. J. Hurd, "Report on End of Cycle 52 Documentation," Los Alamos National Laboratory internal report (October 1988).
2. J. Guyard and M. Weiss, "Use of Beam Emittance Measurement in Matching Problems," in Proceedings of the 1976 Proton Linear Accelerator Conference, Atomic Energy of Canada Limited report, AECL-5677 (November 1976), p. 255.
3. K. Crandall, "TRACE 3-D Documentation," Los Alamos National Laboratory report LA-11054-MS (August 1987).